Environmental study of a Micromegas detector

C. Adloff, M. Chefdeville, A. Espargilière, R. Gaglione

LAPP-TECH-2009-03
April 24, 2009

Environmental study of a Micromegas detector

C. Adloff, M. Chefdeville, A. Espargilière, R. Gaglione

LAPP - Université de Savoie - CNRS/IN2P3
BP. 110
F-74941 Annecy-le-Vieux Cedex, FRANCE

Environmental study of a Micromegas detector

C. Adloff, M. Chefdeville*, A. Espargilière, R. Gaglione

26/04/2009

We report on measurements of the basic performance of a Micromegas detector for a digital hadronic calorimeter. Electron collection efficiency, energy resolution and gas gain were measured in various mixtures of Ar and CO_2. Also the dependence of the gain on environmental variables (pressure, temperature), gas parameters (flow, mixing ratio) and geometry (amplification gap size) is studied. Eventually, predictions on the impact of these variables on the detection efficiency of thin Micromegas detectors are drawn.

1 Introduction

1.1 Calorimetry at a future electron collider

Several important physics measurements that could be realized at a future electron linear collider (ILC or CLIC) would require a very good jet energy resolution (3 % at 100 GeV) [1]. The Particle Flow Approach (PFA) has been proposed to reach such a resolution. It consists in measuring the energy of the each particle contained in a jet with the tracker or with the calorimeters depending on its charge. While charged particle energy is measured with the tracker (which is more precise than the calorimeters), neutral particle energy is deduced from the energy deposit in the calorimeter from which the contribution of charged particles is subtracted. This calls for finely segmented calorimeters with single shower imaging capability.

A digital hadronic calorimeter (DHCAL) is a candidate at a future linear collider which would balance the cost of an increased number of readout channels (with a cell size of 1 cm^2 and a total active area of $3{\cdot}10^3$ m^2, $3{\cdot}10^7$ cells should be read out) by a simpler readout circuitry (1 bit information). The energy of a hadron would then be measured by summing up the hits, taking into account the calibration constant of the detector. A DHCAL can be instrumented with scintillating or gaseous layers. In the latter case, GEMs, RPCs and Micromegas are being considered [2, 3, 4]. Some benefits of a Micromegas DHCAL are a potentially high efficiency for MIPs, a low hit multiplicity (close to 1) [4], low working voltages (400-500 V which is low w.r.t. GEMs and RPCs), a thin sensitive layer (3 mm of Ar), a very good long-term irradiation behaviour and a high rate capability (no gain saturation up to GHz/mm^2 with thin gas layers) [5]. A disadvantage of thin gap Micromegas is the small charge that the readout circuits have to accommodate (a few tens of fC for a MIP).

*author e-mail: chefdevi@lapp.in2p3.fr

1.2 Detection efficiency of a Micromegas DHCAL

The performance of a Micromegas DHCAL (single particle energy resolution and shower separation capability) should depend on the detection efficiency and the hit multiplicity. We derive here a simple formula for the detection efficiency as a function of signal and threshold. This will motivate the study of the gain sensitivity to various parameters.

For a given electronic threshold t and total charge distribution on a pad $p(Q_\mathrm{t})$, the efficiency η can be simply expressed as:

$$\eta = \int_t^\infty p(Q_\mathrm{t}) dQ_\mathrm{t} \tag{1}$$

where the distribution $p(Q_\mathrm{t})$ is normalized. It is the convolution of the primary charge distribution $p(Q_\mathrm{p})$ and the gas gain distribution $p(G)$. For a charged particle of given energy, a parametrization of $p(Q_\mathrm{p})$ is the Landau distribution [6]. The gas gain distribution is generally assumed to be a decreasing exponential distribution [7]. Eventually, $p(Q_\mathrm{t})$ can also be described by a Landau distribution.

The solution of Equation 1 is not known but can be calculated by numerical integration. For this purpose, the two parameters of the Landau distribution $p(Q_\mathrm{t})$ (most probable value MPV and a scale parameter) are deduced from the analysis of data recently collected in a beam test at CERN (200 GeV muons traversing mostly at normal incidence 3 mm of $\mathrm{Ar}/i\mathrm{C_4H_{10}}$ 95/5). The Landau distribution as adjusted to the measurements is shown in Figure 1 (a). The calculated efficiency as a function of threshold is shown in Figure 1 (b).

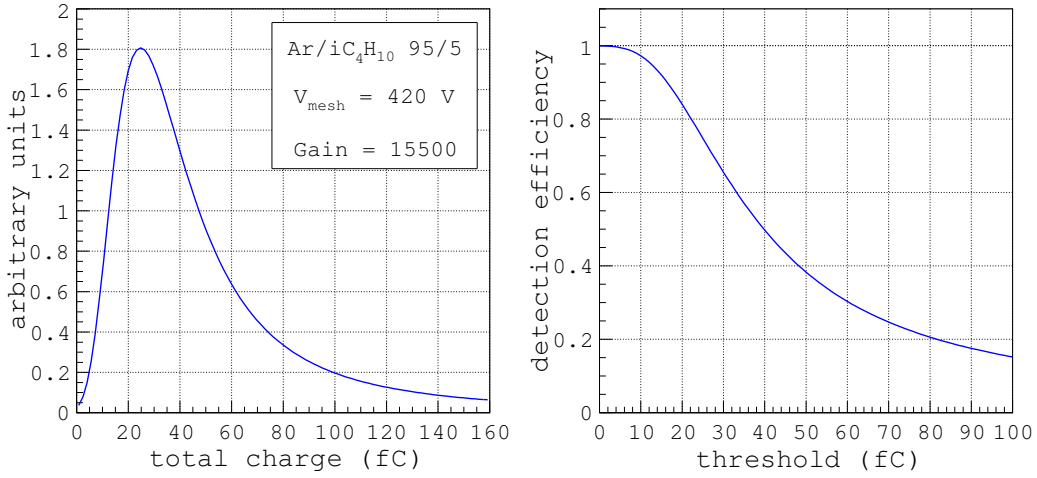

(a) (b)

Figure 1: *Landau distribution fitted to beam test data (a). Calculated detection efficiency as a function of threshold (b). These results are for 200 GeV/c muons traversing 3 mm of* Ar/iC_4H_{10} *95/5.*

Using these results, the efficiency of HARDROC [8] or DIRAC-based [9] Micromegas chambers can be predicted. Assuming an electronic threshold of 20–30 fC, the efficiency would lie between 0.6–0.8. Still, this figure applies for 200 GeV/c muons which are 50 % more ionising than true MIPs (300 MeV/c muons): the efficiency for MIPs would be worse.
For a DHCAL, the efficiency should be as high as possible. Because the MPV is proportional to the gas gain, the gain sensitivity to changes in, for instance, pressure should be known. In particular the drop of gain due to a given increase of pressure or decrease of temperature should be quantified.

In the next section we discuss some variables that impact on the gain. The purpose of our study is to measure (or predict) how sensitive the gain is to variations of each of them. Gain variations can be measured relatively simply by monitoring the signal from ^{55}Fe quanta conversion in the gas. Indeed, variations of Q_{t} are a direct indication of gain variations because the energy absorbed in the gas is fixed in this case (in opposition with traversing charged particles). The experimental setup is described in section 3 and the measurements are reported in sections 4 and 5. As a conclusion, an attempt is made to predict efficiency variations from gain variations.

2 Gas gain variations

2.1 Gas and environmental variables

The following variables impact on the gas gain:

- atmospheric pressure. Our detector is constantly flushed with a mixture of gas, the gas pressure variations hence follow atmospheric pressure variations. When the pressure decreases, so is the gas molecular number density: avalanche electrons get more energy between collisions with the gas molecules and the fraction of ionizing collision increases. At the same time, the mean distance between ionisation increases (because the ionisation cross section and the gas number density decrease). As a result, there is a maximum of gain as a function pressure. The pressure at which the gain is maximum depends on the temperature and the amplification gap thickness [12];

- gas temperature. Similarly to the pressure, the temperature impacts on the molecular number density and thus on the gain. According to the ideal gas law, the number density is $n = P/(k_{\mathrm{B}}\,T)$;

- amplification gap size. Gap variations affect the gain uniformity over the mesh area and depend on the fabrication process of the Bulk Micromegas. At given grid voltage, pressure, temperature and in a given gas mixture, the number of ionising collisions per unit path (so-called Townsend coefficient α) depends on the field strength. Hence, the gain depends on the field and the gap size g: $G = \exp(\alpha g)$. Similarly to the pressure dependence, the gain exhibits a maximum as a function of gap: in Ar-based mixtures this gap was measured to be close to 55 μm [10]. Above this value, the gain is a decreasing function of gap as the lower field does not compensate for the larger distance available for the avalanche development;

- gas mixing ratio. Proportional gas detectors are operated in a mixture of a noble and a molecular gas (so-called quencher). When the mixture is made with mass flow controllers, the relative concentrations of the two species may change. Quencher gases efficiently absorb the electron energy because of vibration and rotation modes available at low energy (a few tenth to a few eV) [13]. As a result, for quencher concentration above a few percents the gain decreases with the quencher concentration ([15]);

- gas flow. At low flow, the concentration of electronegative impurities (*e.g.* O_2, H_2O) may be responsible for signal loss by electron attachment. The attachment cross-section of a given electronegative species depends on the electron energy and thus the field strength. It may thus happen in the drift or amplification region.

As will be shown in the next section, the functional dependence of the gain on the grid voltage, gap size and P, T variables is similar.

2.2 Gas gain model

In this section a parametrization of the gain in terms of the variables of interest is proposed. The parameters will be deduced from two independent measurements: gain as a function of grid voltage (section 4) and gain, pressure and temperature as a function time (section 5).

The gain is equal to the exponential of the number of ionisation produced by the avalanche initiating electron:

$$G = \exp(\alpha g) \tag{2}$$

where α is the number of ionisation per unit distance (so-called Townsend coefficient) and g is the amplification gap size. A common parametrization of α was proposed by Rose and Korff [14]:

$$\alpha/n = A_0 \exp(-B_0 n/E) \tag{3}$$

with n the gas number density and A_0, B_0 two constants that depend on the gas. Writing N_{A} the Avogadro's number and R the ideal gas constant, the gas number density can be expressed as:

$$n = \frac{N_{\mathrm{A}} P}{RT} \tag{4}$$

Combining Equations 2–4:

$$G = \exp\left(\frac{APg}{T}\exp(-\frac{BPg}{TV})\right) \tag{5}$$

where A and B depend on the gas mixture and V is the mesh voltage ($V = Eg$). According to Equation 5 the gain goes through a maximum for:

$$\left(\frac{Pg}{T}\right)^{*} = \frac{V}{B} \tag{6}$$

which is the well-known property of Micromegas (and more generally of any parallel plate detector working in proportional mode) that at a given voltage and in a given gas mixture, the gain goes through a maximum for a particular set of gap, pressure and temperature [12]. At NTP in Ar/CH_4 90/10 and Ar/iC_4H_{10} 80/20, this maximum was measured for a gap of about 55 μm [10, 16], the mesh voltage was about 400 V. Measurements of gain as a function of pressure in Ar/C_6H_{12} 93/7 at V = 270 V shown that the gain goes through a maximum at a pressure of 500–550 mbar [12].

The gain sensitivity to changes in ambient variables or gap size can be calculated from Equation 5:

$$\frac{\Delta G}{G} = C_{\mathrm{P}}\Delta P + C_{\mathrm{T}}\Delta T + C_{\mathrm{g}}\Delta g \tag{7}$$

where

$$C_{\mathrm{P}} = \frac{1}{G}\cdot\frac{\partial G}{\partial P} = \exp(-\frac{BPg}{TV})\cdot(\frac{Ag}{T} - \frac{ABPg^2}{T^2V}) \tag{8}$$

$$C_{\mathrm{T}} = \frac{1}{G}\cdot\frac{\partial G}{\partial T} = \exp(-\frac{BPg}{TV})\cdot(\frac{ABP^2g^2}{T^3V} - \frac{APg}{T^2}) \tag{9}$$

$$C_{\mathrm{g}} = \frac{1}{G}\cdot\frac{\partial G}{\partial g} = \exp(-\frac{BPg}{TV})\cdot(\frac{AP}{T} - \frac{ABgP^2}{T^2V}) \tag{10}$$

The parameters A and B will be deduced from gas gain measurements in section 4 and used to calculate $(Pg/T)^{*}$, C_{P}, C_{T} and C_{g}. In section 5, C_{P} and C_{T} are measured and compared with their calculated values.

3 Experimental setup

3.1 Chamber

The test chamber is formed by a 6×16 cm^2 anode plane segmented into 96 pads, a Micromegas mesh maintained 128 μm above the anode PCB by insulating pillars (so-called Bulk Micromegas [17]), a 3 mm thick plastic frame which defines the drift region and a grounded steel cover. The drift electrode is a copper foil glued on a kapton, itself glued on the cover inside surface. The cover is perforated in some spots for X-ray characterization. The gas is flushed in the chamber through two holes in the plastic frame.
This chamber is part of a stack of four chambers (Figure 2) built for efficiency and multiplicity studies in beam tests [4]. Among the four chambers, only one is used for our measurements.

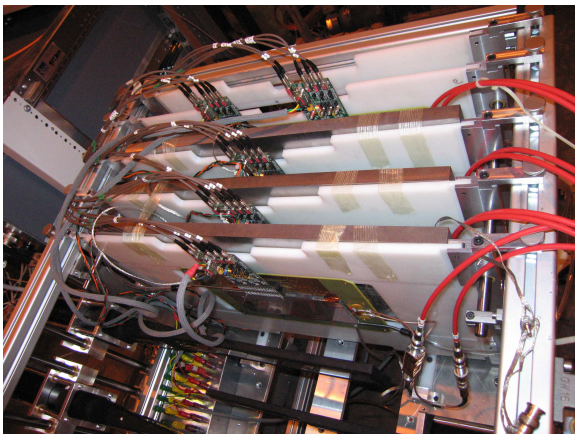

Figure 2: Photograph showing the stack of four Micromegas chambers.

3.2 Gas system

The gas system consists of two bottles of Ar and CO_2, two mass flow controllers, a mixing barrel, four rotameters and bumbles (with the four chambers in between) and one exhaust. The mass flow controllers are calibrated for the two gas species. The Ar and CO_2 controllers deliver a maximum flow of 3 and 0.96 l/h respectively. The flow can be controlled to a 1 % accuracy. A third controller calibrated for iC_4H_{10} is available but not used.

The rotameter valves are opened completely and can be used to measure the gas flow and check that it complies with the controller settings. A good agreement was found up to gas flows of 1.5 l/h above which the rotameter measurement saturates. This may be an indication of a leak between the controllers and the rotameters. In typical working conditions the flow rate is about 1 l/h so we are confident that the mixing ratio in the chamber is precisely known.

3.3 Signal readout and DAQ

Each primary electron from ^{55}Fe conversions reaching the amplification region initiates an avalanche. The motion of avalanche electrons and ions in the gap induces a signal of opposite polarity on the

pad underneath and the mesh. The signals from individual avalanches are picked up on the mesh by an ORTEC preamplifier, followed by an ORTEC amplifier/shaper. The output pulse is digitized by a 12 bit VME ADC housed in a crate. A fast output of the ORTEC preamplifier is used to trigger the digitization when the pulse amplitude is maximum. The ADC is read by the CENTAURE program which takes care of spectrum display and saving. The calibration constant of the readout chain was precisely measured to be 2.199 ± 0.026 ADU/fC (where ADU stands for ADC Units) [18].

The CENTAURE acquisition settings, source activity and collimation are such that the event rate is about 100 Hz and that 1 MBytes files are written every 10–30 minutes depending on the gas pressure. Each file contains about 50000 events. In parallel to that, a slow control of the atmospheric pressure, chamber over-pressure and gas temperature is done. These variables are written to file every 100 seconds.

3.4 Data analysis

The analysis consists in reconstructing ^{55}Fe spectra of 10^4 events and determining the position and width of the photopeak. This is realized by fitting the parameters of a dedicated function to the spectra. The function is the sum of three gaussians: one accounting for the escape peak, two for the K_α and K_β lines of the photopeak (an ^{55}Fe source emits 5.9 and 6.5 keV photons in the ratio 8.5/1 [11]). The parameters of the K_β peak are fully constrained by the K_α ones:

$$\mu_\beta = \mu_\alpha \frac{6.5}{5.9} \tag{11}$$

$$\sigma_\beta = \sigma_\alpha \sqrt{\frac{6.5}{5.9}} \tag{12}$$

$$h_\beta \sim \frac{h_\alpha}{7} \tag{13}$$

where μ, σ and h are the mean, standard deviation and maximum of a gaussian. Finally the number of free parameters reduces to 6: half for the escape peak, half for the photopeak. A measured spectrum with the fitted function is shown in Figure 3.
In the next two sections we present measurements of some basic properties of the Micromegas used in Ar/CO_2 and results of the environmental study in Ar/CO_2 80/20.

4 Micromegas basic properties in Ar/CO_2 mixtures

4.1 Electron collection efficiency

The electron collection efficiency is the probability that a primary electron enters the amplification region. It depends mainly on the field configuration and to a lower extend on the electron transverse diffusion. In Micromegas the electron collection improves with the compression of the field lines from the drift to the amplification region. The compression factor (more precisely the ratio of the funnel cross section areas at the drift electrode and at the anode S_D/S_A) is equal to the ratio of the fields (E_A/E_D). Accordingly, at a given grid voltage (E_A constant) the collection efficiency increases when lowering the drift field. Above a certain field ratio, the collection efficiency may be close to 1 as all electrons should enter the amplification region.

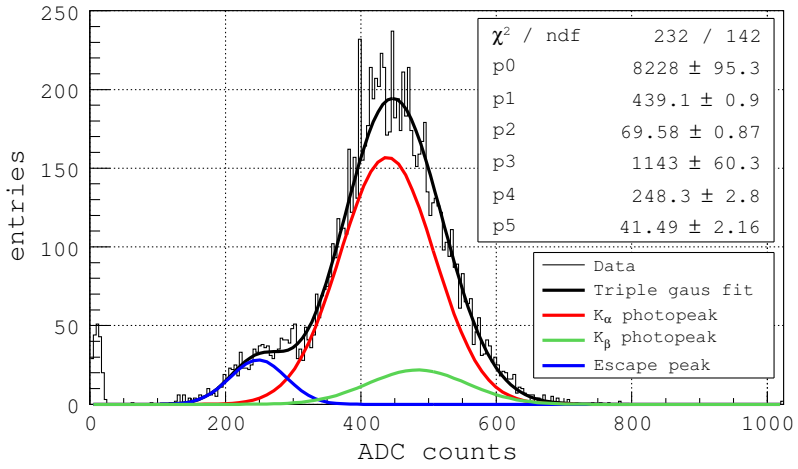

Figure 3: ^{55}*Fe spectrum in Ar/CO$_2$ 80/20 at* V_{mesh} *= 570 V.*

The ^{55}Fe photopeak position was measured as a function of drift field in Ar/CO$_2$ mixtures. In each mixture, the mesh voltage is adjusted so as to have signals of similar magnitudes: V_{mesh} = 485 V, 520 V and 570 V in Ar/CO$_2$ 5/95, 90/10 and 80/20 respectively. The measurements are shown in Figure 4.

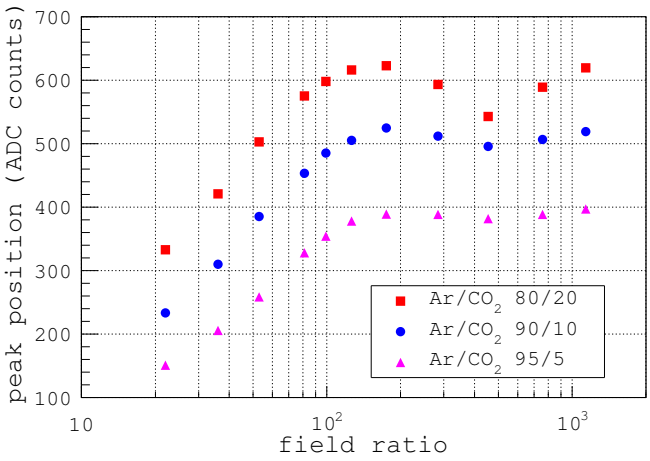

Figure 4: ^{55}*Fe photopeak position and field ratio in Ar/CO$_2$ mixtures.*

It is observed that the peak position first rises with the field ratio (*FR*) as the collection efficiency improves. Instead of the expected plateau the position then decreases above *FR* = 200, reaches a local minimum at *FR* = 500 and rises again. This trend is observed for the three gas mixtures and is more pronounced at larger CO$_2$ fractions. It can be explained by attachment of some primary electrons in the drift region by electronegative impurities. This explanation is supported

by the fact that the local minimum is reached at similar values of the drift field ($E_{\mathrm{D}} = 75$–90 V/cm). Attachment in mixtures containing a significant fraction of CO_2 is a three-body process that involves oxygen molecules [7]: the attachment probability depends on the CO_2 and O_2 concentration. Hence, if our explanation is correct the dip may disappear if the gas tightness of the chamber is improved.

The maximum of the signal is obtained at a field ratio of 200 which corresponds to drift fields of 190, 203 and 223 V/cm in Ar/CO_2 95/5, 90/10 and 80/20. At such field ratios, the collection efficiency may be maximum.

4.2 Gas gain

The gas gain is calculated from the measured peak position, the known calibration constant of the readout chain (cf. section 3.3) and the expected number of primary electrons in the gas mixture. Using W from literature ($W(\mathrm{Ar}) = 25.6$ eV and $W(CO_2) = 36.0$ eV [19]), a simple weighted average (which neglects the different values of the ionisation cross section of Ar and CO_2) yields 221, 219 and 212 electrons in Ar/CO_2 95/5, 90/10 and 80/20. At a drift field of 30 V/cm, the peak position is measured as a function of grid voltage until the spark rate reaches about 0.1 Hz. The pressure variation throughout the measurement period is 2 mbar. The measurements corrected for this variation are shown in Figure 5.

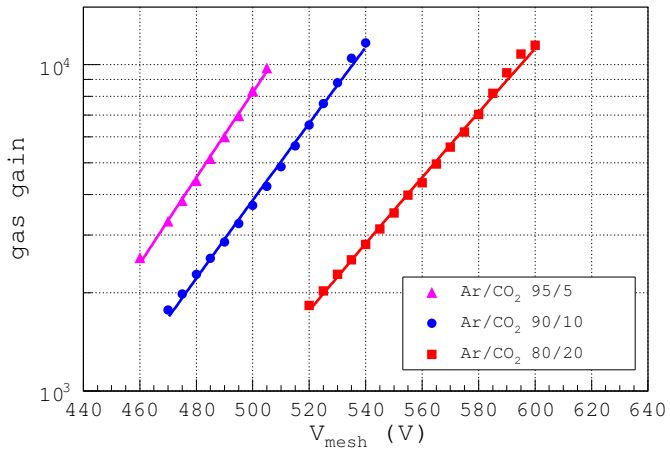

Figure 5: *Gas gain of a 128 μm gap Micromegas in Ar/CO_2 mixtures.*

As expected the gain decreases with the CO_2 fraction. The maximum gain is about 10^4 in Ar/CO_2 80/20 and 90/10 and slightly lower in the 95/5 mixture probably due to a poorer quenching.

The parameters of Equation 5 are adjusted to the measured $G(V)$ trend for each mixture and are listed in Table 1. The other variables that enter Equation 5 were fixed to $P = 963$ mbar, $T = 298$ K and $g = 128$ μm (P and T were measured, g is assumed equal to the pillar thickness). The calculated $(Pg/T)^*$, C_{P}, C_{T} and C_{g} (Equations 6–10) appear in Table 2. In Ar/CO_2 80/20, they are equal to -0.5, 1.5 and -3.5 % respectively. These figures decrease with the quencher fraction (or increase with the steepness of the gain curve).

Mixing ratio	$A \pm \Delta A$ (K/mbar/μm)	$B \pm \Delta B$ (V·K/mbar/μm)
80/20	0.097 ± 0.002	2.12 ± 0.02
90/10	0.110 ± 0.002	2.06 ± 0.02
95/5	0.121 ± 0.003	2.07 ± 0.03

Table 1: *Parameters A and B of Equation 5 adjusted to the measured gain curves in Ar/CO_2 mixtures.*

Mixing ratio	C_{P} (1/mbar)	C_{T} (1/K)	C_{g} (1/μm)	$(Pg/T)^*$ (mbar·μm/K)	g^* (μm)
80/20	-0.46	1.50	-3.49	273	84
90/10	-0.59	1.91	-4.44	281	87
95/5	-0.68	2.18	-5.08	280	87

Table 2: *Gain relative variation in % for changes in pressure, temperature and gap size. The quantity $(Pg/T)^* = V/B$ is calculated for a grid voltage yielding a gain of 5600 (e.g. 570 V in the 80/20 mixture). The gap g^* is calculated at 963 mbar and 298 K.*

4.3 Energy resolution

The energy resolution of our proportional chamber to ^{55}Fe signals is governed by primary charge fluctuations, electron collection efficiency, gain fluctuations and electronic noise. Assuming full collection, the resolution R can be expressed as:

$$R = \sqrt{\frac{W(F+b)}{E_0} + R_{\mathrm{n}}} \tag{14}$$

where E_0 is the energy absorbed in the gas, F the Fano factor, b the relative variance of the gain distribution and R_{n} the contribution from the noise. Using $F = 0.2$ [10], $b = 0.5$ [20], $W = 27$ eV, the theoretical limit of the resolution at 5.9 keV in Ar/CO_2 mixtures is about 5.6 % r.m.s..

For every measured ^{55}Fe spectrum, the resolution is calculated as the relative width of the photopeak. The trend of the resolution as a function of gas gain is shown in Figure 6. The measured resolution is equal to 11–15 % which is twice larger than the theoretical limit which can be explained by the important noise at the preamplifier input. The latter results from the detector capacitance which due to the large mesh area is high ($C_{\mathrm{detector}}(96\ \mathrm{cm}^2) \sim 0.5$–1 nF, neglecting the pillar dielectric permittivity).

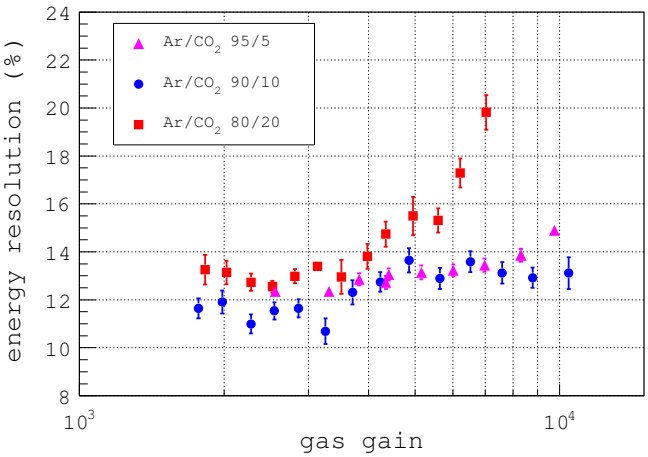

Figure 6: *Energy resolution at 5.9 keV and gain in Ar/CO_2 mixtures.*

5 Environmental study

5.1 Signal and gas flow

The study of the signal dependence on gas flow was conducted prior to the installation of the mass flow controllers. The ^{55}Fe photopeak position was measured in a mixture of Ar/iC$_4$H$_{10}$ 95/5 available from a pre-mixed bottle. In that configuration, the mixture was flushed through the rotameters and the chambers. The rotameters were calibrated for that mixture and were used to change the flow between 0.05 and 0.3 l/h. The measurements are shown in Figure 7.

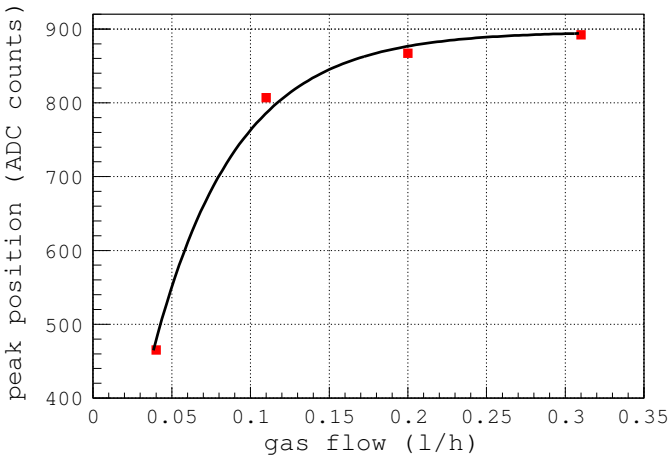

Figure 7: ^{55}*Fe photopeak position in Ar/iC_4H_{10} 95/5 and gas flow through four chambers placed in parallel. The volume of the chamber of interest is equal to 0.03 l and the total volume of the four chambers is 0.2 l.*

The peak position increases with the flow probably because of a decrease of the concentration of electronegative impurities inside the chamber. It is not clear if it is the gain or the collection efficiency or both that increase with the flow. Still, we observe that the peak reaches a stable value for flows larger than 0.25–0.3 l/h. As the gas is flushed through three chambers of 0.029 l and one of 0.115 l the effective flow through the chamber of interest is one seventh of the flow indicated in Figure 7 (assuming the same gas tightness for all chambers). Accordingly, the saturation is reached for a flow of 1.2–1.5 chamber volume per hour.

5.2 Two week study

During two weeks the amplitude of some 10^8 pulses from ^{55}Fe quanta conversions in Ar/CO_2 80/20 were recorded, enabling a precise monitoring of the detector gain as a function of time. In parallel, gas pressure and temperature were also recorded. The grid voltage is set to 570 V at which a gain of about $5{\cdot}10^3$ is expected. The drift field is kept at 100 V/cm which corresponds to a field ratio of 445. The Ar and CO_2 gas flows are equal to 0.97 and 0.24 l/h, yielding a total flow of 1.21 l/h.

The trends of the peak position, gas pressure and temperature as a function of time are shown in Figure 8 (a)–(c). The three peaks in the temperature trend at 1.6 and 4.8 and 5.0 days result from a voluntary change of the room temperature by means of an air conditioner. After 5.2 days, the room windows were masked to prevent sun light from reaching our setup. As a result, the temperature variations are significantly reduced.
The data analysis is based on the assumption that the gain dependence on the pressure P and the temperature T are independent. Hence, we first measure $G(P)$ when the temperature varies little and correct $G(t)$ for pressure variations. The corrected variations of $G(t)$ should then be caused by temperature variations only and the relation $G(T)$ can be determined.

5.3 Gain and gas pressure

Ideally the gain dependence on pressure should be determined at constant temperature. In our case, the temperature changes with time and therefore the gain and pressure variations should be studied over small temperature ranges (*e.g.* $\Delta T = 0.1$ °C). On the other hand, the relation $G(T)$ will be more accurately studied if one allows for a larger ΔT because the pressure variations ΔP will be larger. Accordingly we chose a temperature range of 1 °C which is the largest variation measured between 5.2 and 16 days.
A scatter plot of peak position (proportional to gain) and pressure measured during this time is shown in Figure 9 (a) (T = 24.5–25.5 °C). According to Equation 5, we use the following parametrization:

$$G(P) = \exp(A_1 P \exp(-B_1 P)) \tag{15}$$

with

$$A_1 = \frac{Ag}{T} \tag{16}$$

and

$$B_1 = \frac{Bg}{TV} \tag{17}$$

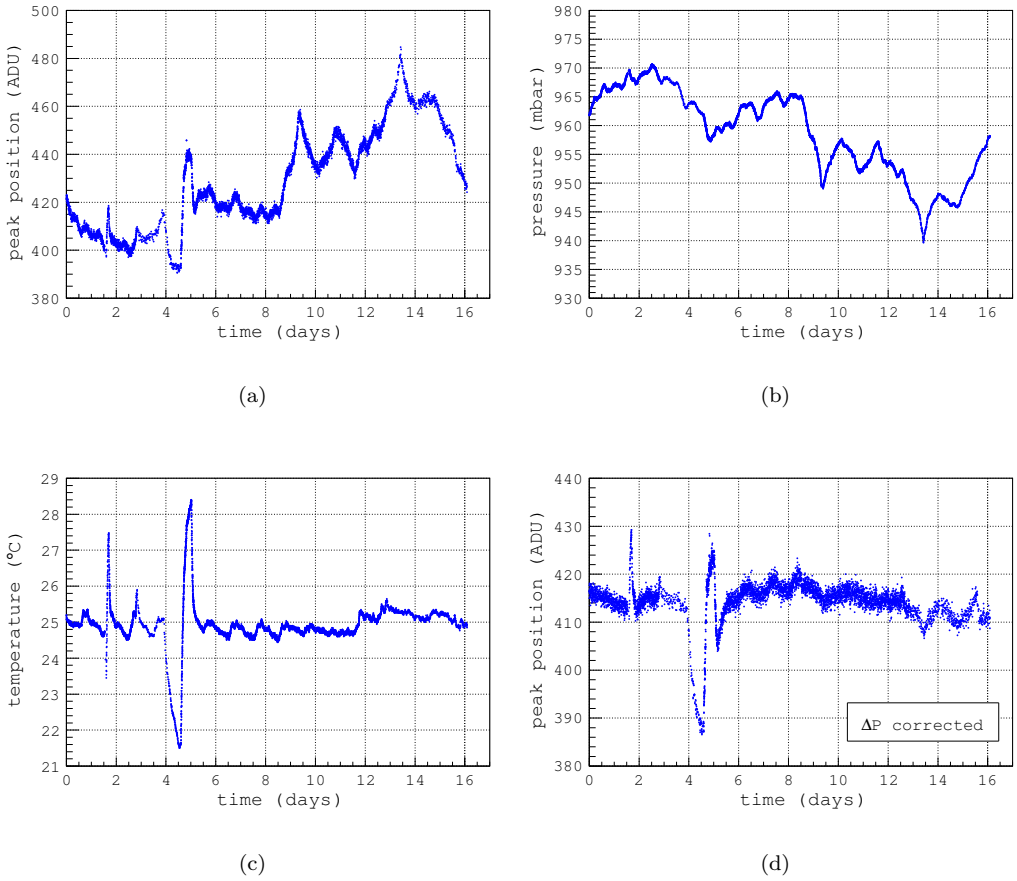

Figure 8: ^{55}*Fe photopeak position (a), pressure (b) and temperature (c) as a function of time. Peak position corrected for pressure variations as a function of time (d) (cf. section 5.4).*

Adjusting A_1 and B_1 to the data points, we find $A = 0.11$ K/μm/mbar and $B = 2.34$ KV/μm/mbar which are compatible with the values determined from the gain curve[1]. Accordingly, the relative gain variation for a pressure change of 1 mbar is C_{P} = -0.63 %/mbar (cf. Equation 8). This is in good agreement with the gain curve calculated value of -0.46 %/mbar.

5.4 Gain and temperature

The peak position p (or gain) at a time t is corrected for pressure variations using Equation 7:

$$p_{\mathrm{cor}}(t) = p(t_0) + \Delta p(t) \sim 13.4 \cdot (G(t_0) + \Delta G) \sim 13.4 \cdot G(t_0)(1 + C_{\mathrm{P}} \Delta P) \qquad (18)$$

[1]The parameters A_1 and B_1 relates to the parameters p_0 and p_1 of Figure 9 through a calibration constant: $G \sim 13.4 \cdot ADU$

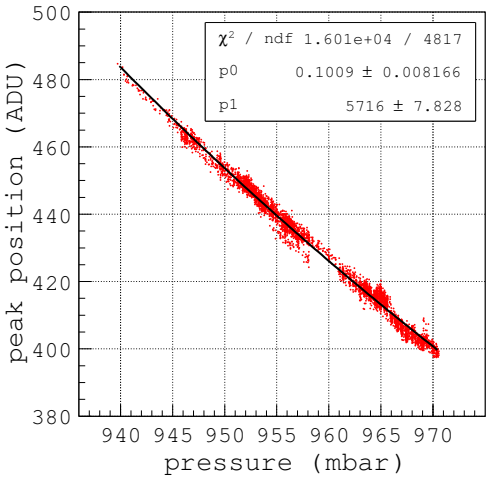

Figure 9: ^{55}*Fe photopeak position and pressure measured between 5.2 and 16 days.*

The obtained trend of $p(t)$ is shown in Figure 8 (d) where the peak variations should be caused by changes of temperature only. A scatter plot of the pressure corrected peak position and temperature is shown in Figure 10. This graph includes data collected between 4.0 and 5.1 days when the temperature variations were the largest. Using Equation 5:

$$G(T) = \exp(A_2/T \exp(-B_2/T)) \tag{19}$$

and fitting A_2 and B_2 to the data, we obtain $A = 0.11$ K/μm/mbar and $B = 2.33$ KV/μm/mbar. The gain relative sensitivity to temperature variations is thus $C_{\mathrm{T}} = 2.01$ %/K (Equation 9) which agrees relatively well with the value of 1.50 %/K deduced from the gain curve.

5.5 Gain and amplification gap size

The measurement of the gain sensitivity to gap variations is difficult as it requires Micromegas of various gap sizes. Such a measurement could be performed with three integrated Micromegas (so-called InGrid detectors) of gap sizes ranging from 45 to 70 μm [10, 16], showing that in Ar-based mixtures at NTP and at a voltage of 390–440 V the gain is maximum for a gap size of about 55 μm. This study can not be performed here, nevertheless the gain sensitivity to gap variations can be predicted using the values of A and B deduced from the gain curve or from the environmental study. At a pressure of 963 mbar, a temperature of 298 K, a grid voltage of 570 V and for a gap size of 128 μm, the gain sensitivity to gap size variation C_{g} lies between 3.5–4.7 %/μm.

The gap size uniformity of our Bulk Micromegas is not precisely known but is probably in the order of one to a few microns. Therefore the gain should vary at least by a few percents across the mesh area. This prediction can be put to the test if several measurements of the gain across the mesh area are performed. These are not available yet, however, they should be done with the 32×48 cm^2 ASU test box (perforated aluminium cover).

Another prediction concerns the product $(Pg/T)^*$ for which the gain (at a given mesh voltage and in a given gas mixture) is maximum. Using the measured value of $B = 2.12$ KV/μm/mbar

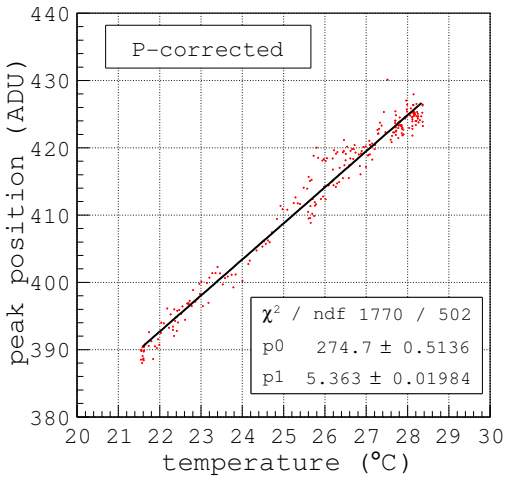

Figure 10: ^{55}*Fe photopeak position corrected for pressure variations as a function of temperature measured between 4.0 and 5.1 days.*

we find at 570 V: $(Pg/T)^* = 268$ K/μm/mbar which yields an optimum gap of 83 μm at NTP. To reach this optimum with our current gap size of 128 μm and at room temperature, a pressure of 635 mbar or a working voltage of 880 V would be needed. The optimum working point can not therefore be obtained with our detector [2].

5.6 Gain and gas mixture

When two gases from different bottles are mixed, variations of their concentrations and hence of the gain can occur. The gain sensitivity to quencher fraction variations was determined by changing the CO_2 fraction from 20 % down to 12 % by small steps of 2 % and measuring a gain curve. The measurements were carried out over two days and are shown in Figure 11. For each mixture the gain is corrected for pressure and temperature, taking 958 mbar and 298 K as reference conditions. The gain at a mesh voltage of 550 V is plotted as a function of the CO_2 fraction in Figure 12.

The trend is well described by a decreasing exponential function and we use the following parametrization to calculate the sensitivity:

$$G(f) = \exp(A_3 + B_3 f) \tag{20}$$

where f stands for the CO_2 fraction. Adjusting A_3 and B_3 to the data points we obtain $(B_3 \pm \Delta B_3)$ = (-0.177 ± 0.004) /% from which the gain sensitivity is:

$$\frac{\Delta G}{G} = -0.177 \Delta f \tag{21}$$

Accordingly, in Ar/CO_2 mixtures with a quencher fraction between 12–20 %, an absolute variation of 1 % of the relative concentrations results in a gain variation of about 18 %. During the two

[2] With a mesh voltage of 880 V, we have $(Pg/T)^* \sim 415$ which yields an optimum gap of 128 μm at NTP. This voltage, however, is not reachable in practice because of the onset of sparks.

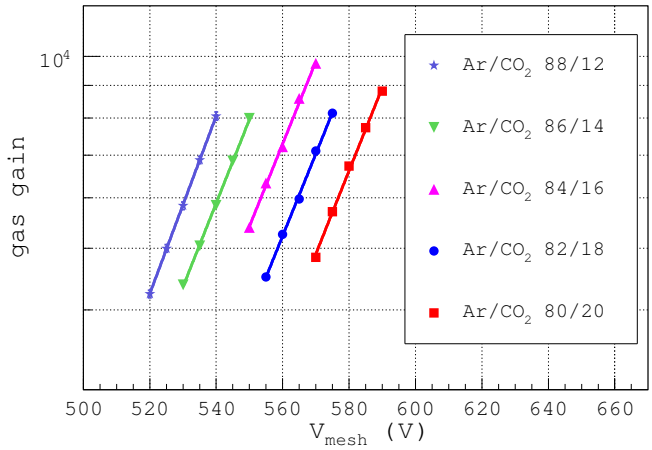

Figure 11: *Gain curves measured in various Ar/CO_2 mixtures at 958 mbar and 298 K.*

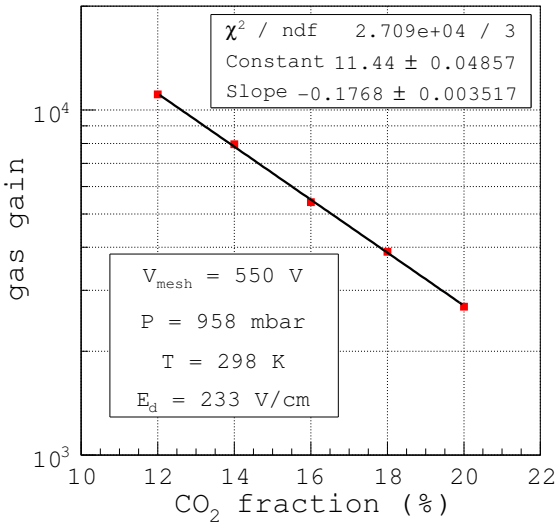

Figure 12: *Gas gain at a grid voltage of 550 V in various Ar/CO_2 mixtures.*

weeks of the environmental study the Ar and CO_2 flows slightly changed. The largest measured deviation from the initial 80/20 mixture was 79.94/20.06 (the mixing ratio was measured every day). This should have changed the gain by 1 %. As a conclusion, our gas system delivers a steady mixture. Also, the measurements presented in Figure 8 should be affected very little by such small variations.

6 Conclusion and extrapolation to arbitrary gas gain

6.1 Gain sensitivity to P, T, g and f variations

We investigated the dependence of the gain on various ambient and gas parameters. In particular the pressure and temperature dependence were measured in two independent ways. A good agreement was found between both measurements. In Ar/CO_2 80/20 at a grid voltage of 570 V, we obtained:

$$\frac{\Delta G}{G} \sim -(0.5-0.6)\ \%\ \Delta P + (1.5-2.0)\ \%\ \Delta T - 3.5\ \%\ \Delta g - 17.7\ \%\ \Delta f \tag{22}$$

with ΔP, ΔT, Δg and Δf in millibar, Kelvin, micron and %.

6.2 Impact on the detection efficiency

Considering a gain of 10^4 (grid voltage of 605 V in Ar/CO_2 80/20), NTP and taking realistic changes in pressure, temperature, gap size and CO_2 fraction of 10 mbar, -5 K, 5 μm and 0.5 %, Equations 15 and 21 yield negative gain variations of 6 %, 10 %, 17.5 % and 8.9 % respectively. To calculate the impact on the efficiency an important input is the signal distribution in that gas mixture. It was not measured but can be inferred from that measured in $Ar/i C_4H_{10}$ 95/5 (cf. Figure 1 (a)) assuming that the two parameters of the Landau distribution both scale with the total charge at the anode pads $Q_t = Q_p G$. Because Q_p in $Ar/i C_4H_{10}$ 95/5 and Ar/CO_2 80/20 are similar, we have:

$$\mathrm{MPV}(Ar/CO_2\ 80/20) \sim \mathrm{MPV}(Ar/i C_4H_{10}\ 95/5)\cdot\frac{G(Ar/CO_2\ 80/20)}{G(Ar/i C_4H_{10}\ 95/5)} \sim 29\ \mathrm{fC}\cdot\frac{10^4}{1.5\cdot 10^4} \sim 19\ \mathrm{fC} \tag{23}$$

The trend of the detection efficiency with the Landau distribution MPV (in unit of threshold) calculated by numerical integration of Equation 1 is shown in Figure 13 (a). The ratio MPV/t and the efficiency for various thresholds (from 20 to 60 fC) are listed in Table 3. The efficiency drop due to the mentioned P, T, g and f variations also appear in this Table.

t (fC)	MPV/t	η	η(+10 mbar)	η(-5 K)	η(+5 μm)	η(+0.5 % CO_2)
20	0.95	0.69	0.65	0.63	0.58	0.64
40	0.48	0.33	0.30	0.28	0.24	0.29
60	0.32	0.16	0.14	0.12	0.10	0.13

Table 3: *Effect of pressure, temperature, gap size and CO_2 fraction variation on the efficiency in Ar/CO_2 80/20 at a gain of 10^4 (MPV = 19 fC) for various thresholds.*

We observe that even with a threshold of 20 fC the efficiency is not so high ($\sim$ 70 %) and that the calculated drops are mildly pronounced. In conclusion, the detection efficiency of a Micromegas DHCAL operated in Ar/CO_2 80/20 would be rather insensitive to small changes in pressure, temperature, amplification gap size and CO_2 fraction. However, with a maximum gas gain of 10^4 the efficiency should reach at most 70 % (a minimum threshold of HARDROC and DIRAC chips of

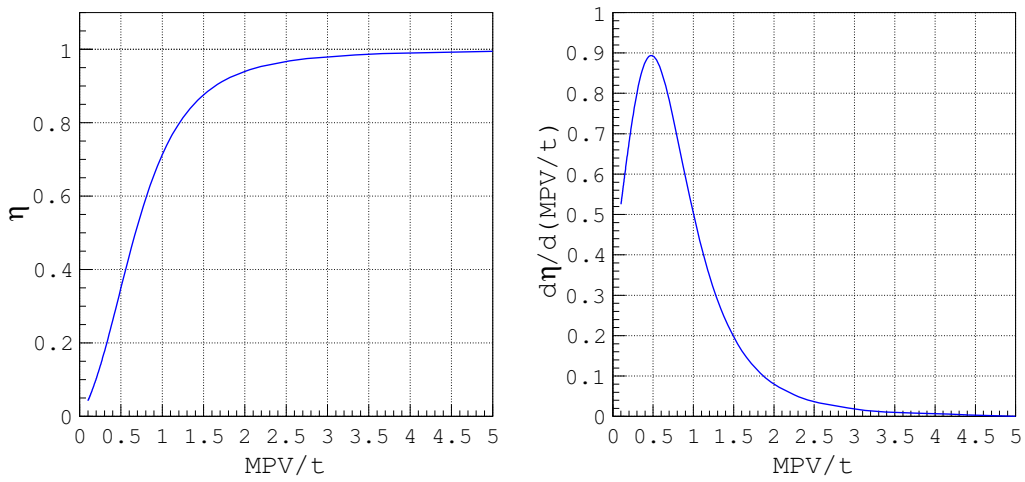

(a) (b)

Figure 13: *Calculated detection efficiency as a function of the Landau MPV in unit of threshold (a) and its derivative (b). The assumption is made that the Landau distribution parameters scale with the gain.*

20 fC is assumed). To increase the efficiency, other gas mixtures with higher maximum gains should be considered.

References

[1] ILC Reference Design Report, Detectors (2007).

[2] J. Yu, GEM DHCal Development, *Proc. of Linear Collider Workshop* DESY, Hamburg (2007).

[3] B. Bilki *et al.*, *JINST* P04006 **4** (2009).

[4] C. Adloff *et al.*, Development of Micromegas for a Digital Hadronic Calorimeter, *Proc. of Linear Collider Workshop* Chicago (2008).

[5] J. Derré *et al.*, *Nucl. Instr. and Meth. A* **412** (1998) 47.

[6] F. Sauli, *Principles of operation of Multiwire Proportional and Drift Chambers* CERN Yellow Reports 77-09 (1977).

[7] W. Blum and L. Rolandi, *Particle detection with drift chambers*, Springer-Verlag Berlin Heidelberg (1993).

[8] V. Boudry *et al.*, HARDROC1, Readout chip of the Digital Hadronic Calorimeter of ILC, *IEEE-NSS conference records* (2007).

[9] R. Gaglione and H. Mathez, DIRAC: a Digital Readout Asic for hAdronic Calorimeter, *IEEE-NSS conference records* **1** (2008) 1815.

[10] M. Chefdeville, *Development of Micromegas like gaseous detectors using a pixel readout chip as collectinganode*. PhD thesis (2009), NIKHEF Institute, Amsterdam, The Netherlands.

[11] Particle Data Group, *Particle Physics Booklet*, (2004).

[12] I. Giomataris *et al.*, *Nucl. Instr. and Meth. A* **419** (1998) 239.

[13] A. Sharma, Properties of some gas mixtures used in tracking detectors, Germany.

[14] J.E. Bateman, Gain stabilisation in proportional counters, RAL-TR-98-044, UK (1998).

[15] I. Krajcar Bronić and B. Grosswendt, *Nucl. Instr. and Meth. B* **142** (1998) 219..

[16] V.M. Blanco Carballo *et al.*, *Nucl. Instr. and Meth. A* **576** (2007) 1.

[17] S. Andriamonje *et al.*, *Nucl. Instr. and Meth. A* **560** (2006) 405.

[18] M. Chefdeville, A. Espargilière and R. Gaglione, Technical note on LAPP LC Detector cosmic bench calibration, LAPP internal document (2009).

[19] L.G. Christophorou, *Atomic and Molecular Radiation Physics*, Wiley, London (1971).

[20] G.D. Alkhazov, *Nucl. Instr. and Meth. A* **89** (1970) 155.